PROCEEDINGS OF SPIE

SPIEDigitalLibrary.org/conference-proceedings-of-spie

Wavefront control experiments with a single mode fiber at the High-Contrast Spectroscopy Testbed for Segmented Telescopes (HCST)

Llop-Sayson, Jorge, Jovanovic, Nemanja, Morrissey, Grady, Echeverri, Daniel, Mawet, Dimitri

Jorge Llop-Sayson, Nemanja Jovanovic, Grady Morrissey, Daniel Echeverri, Dimitri Mawet, "Wavefront control experiments with a single mode fiber at the High-Contrast Spectroscopy Testbed for Segmented Telescopes (HCST)," Proc. SPIE 11443, Space Telescopes and Instrumentation 2020: Optical, Infrared, and Millimeter Wave, 114432Q (13 December 2020); doi: 10.1117/12.2562973

SPIE.

Event: SPIE Astronomical Telescopes + Instrumentation, 2020, Online Only

Wavefront control experiments with a single mode fiber at the High-Contrast Spectroscopy Testbed for Segmented Telescopes (HCST)

Jorge Llop-Sayson[a], Nemanja Jovanovic[a], Grady Morrissey[a], Daniel Echeverri[a], and Dimitri Mawet[a,b]

[a]California Institute of Technology, 1200 E California Blvd., Pasadena, CA 91125
[b]Jet Propulsion Laboratory, California Institute of Technology, 4800 Oak Grove Drive, Pasadena, CA 91109

ABSTRACT

Achieving high levels of contrast over broad bandwidths with segmented aperture telescopes is a key requirement to maximize the scientific yield for future exoplanet imaging missions and ground-based extremely large telescopes. The High-Contrast Spectroscopy Testbed for Segmented Telescopes (HCST) in the Exoplanet Technology Laboratory (ET Lab) at Caltech is designed to proof test new technologies aimed at tackling some of the most pressing and challenging goals of exoplanet science, namely the imaging and spectroscopic characterization of small planets across a wide range of stellar host types, including temperature Earth-size planets. Here we report on the status of a key milestone: Demonstration of 20% bandwidth nulling experiments using single mode fibers wavefront control.

Keywords: High contrast imaging, Exoplanets, Wavefront Control, Wavefront Sensing, Spectroscopy

1. INTRODUCTION

The discovery and characterization of exoplanets toward a complete census of exoplanetary characteristics necessitates of the continuous advancement in direct imaging technologies. The High-Contrast Spectroscopy Testbed for Segmented Telescopes (HCST) at the Caltech Exoplanet Technology Laboratory is specifically designed for this. HCST became operational two years ago[1] and since we have come a long way in developing a most powerful tool to achieve this scientific community's ultimate goals. Last year, we achieved levels of 10^{-8} raw contrast in 10% bandwidth utilizing a System Identification based algorithm to improve the Jacobian calculation.[2] Moreover, we demonstrated the Apodized Vortex Coronagraph concept[3] in high contrast for broadband light. This coronagraph architecture is optimized to deal with segment gaps without the use of the deformable mirrors.[4] In the last months we have been working on performing broadband wavefront control with a single mode fiber (SMF).

The motivation of using SMFs in direct detection of exoplanets comes from enabling higher sensitivity with the mode selectivity provided by an SMF. Indeed, the light from a planet, the position of which is well known, can be injected into an SMF in the image plane, and sent to a high resolution spectrograph to perform high dispersion coronagraphy (HDC).[5,6] Performing wavefront control to reduce the unwanted starlight from coupling into the SMF is a key technology development that will further improve sensitivity to molecular detections in exoplanet's atmospheres with HDC. Furthermore, it has been shown that SMFs allow for wavefront correction over a larger bandpass.[7] For this we use the electric field algorithm (EFC)[8] formalism adapted to an SMF. We previously presented this concept, which was demonstrated for monochromatic light in the prototype version of HCST,[9] and we are currently working on achieving 10^{-8} raw contrast in 20% broadband light.

In these proceedings we present the steps we are taking to achieve this goal. In Sec. 2 we show the laboratory setup, including the changes in HCST's layout to accommodate a fiber injection unit (FIU), and other changes

Send correspondence to J. Llop-Sayson
E-mail: jllopsay@caltech.edu

Space Telescopes and Instrumentation 2020: Optical, Infrared, and Millimeter Wave, edited by Makenzie Lystrup, Marshall D. Perrin, Proc. of SPIE Vol. 11443, 114432Q · © 2020 SPIE
CCC code: 0277-786X/20/$21 · doi: 10.1117/12.2562973

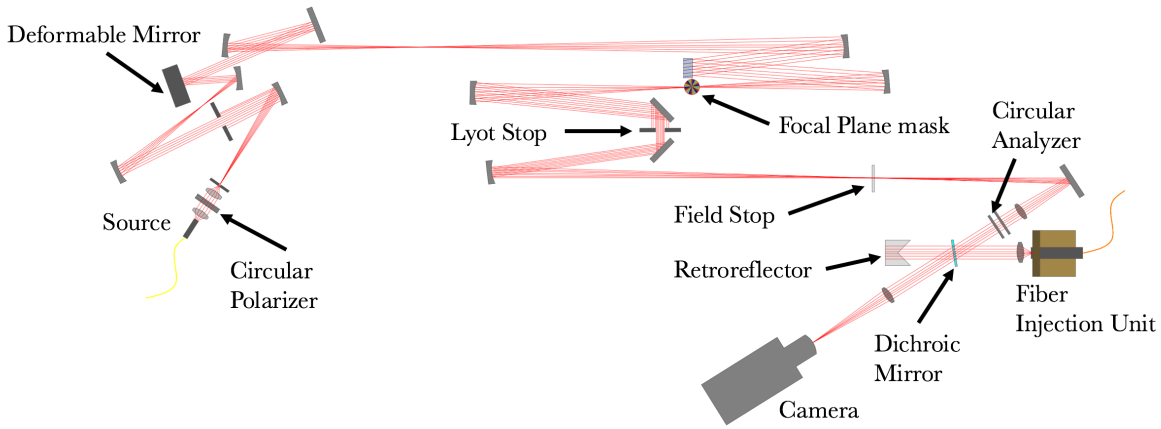

Figure 1. HCST's current layout.

made to boost the testbed's performance. In Sec. 3, we briefly explain the algorithm used to perform wavefront control. In Sec. 4, we show the narrowband results of the SMF wavefront control tests. And in Sec. 5, we present some preliminary results on the broadband SMF nulling tests.

2. LABORATORY SETUP

In this section we describe the current setup of HCST. In Fig.1 we show the layout with its main components. We use a supercontinuum white light source (NKT Photonics SuperK EXTREME) connected to a tunable filter (NKT Photonics SuperK VARIA) from which a single mode fiber (SMF) feeds the light into the testbed. A 5 μm pinhole represents the simulated star, or pseudo-star. We use a Boston Micromachines kilo-DM deformable mirror (DM) with 34×34 actuators. In the apodizer plane we place a flat mirror since we are using an unobstructed open circular aperture. In the focal plane mask (FPM), we use a Vector Vortex Coronagraph.[10,11] The Lyot stop consists of a circular aperture that blocks ∼93% of the radius of the 16.4 mm beam.

Recently added to HCST is the field stop, which is placed in the image plane of the previous camera location. The motivation for adopting this layout comes from the need to avoid ghosts that originate from the bright center of the pseudo-star and the presence of transmissive optics in the beam path, i.e. the circular analyzer that has to be placed in front of the camera, and the protective screen of the camera chip. Besides, the field stop allows us to pick off the light for the FIU with a dichroic mirror after the bright part of the pseudo-star is blocked. The SMF coupling is very sensitive to tip/tilt errors, so the field stop helps to mitigate the unwanted light from the bright part of the pseudo-star introduced by jitter or PSF drift. The manufacturer for the field stop was Shimifrez Inc. For the camera we use an sCMOS (Andor Neo 5.5).

The fiber injection unit allows for the injection of light to a SMF on a precise position in the image plane. The beam is picked with a dichroic mirror at the collimated beam after the field stop and sent to a lens that focuses the light into the SMF image plane. The transmitted light through dichroic mirror goes to the camera, which for the fiber experiments is used as a tracking camera. We control the SMF position with a three-axis stage consisting on three piezo-linear stages from Physik Instrumente (PI Q-545.240). These stages allow for nanometer precision positioning. The retroreflector is used to track the position of the SMF with respect to the camera, and for calibration purposes.

3. EFC WITH A SINGLE MODE FIBER

EFC with an SMF (abbreviated here to EFC-SMF) is an adaptation of the EFC formalism, introduced by Give'On (2009),[8] that accounts for the mode selectivity of an SMF. In conventional EFC, the algorithm iteratively reduces the unwanted starlight in a region in the image plane; when working with a camera, EFC finds a DM solution

that minimizes the intensity in a given set of pixels. In the case of EFC-SMF, the measured output of the SMF is not the intensity at the image plane in the position of the SMF but the overlap integral of the electric field, E_{im}, multiplied by the fundamental mode of the fiber, Ψ_{SMF}:

$$I_{SMF} \propto \left| \int E_{im} \Psi_{SMF} da \right|^2 , \tag{1}$$

We thus aim at minimizing this overlap integral, and not the intensity. Indeed, we are unconcerned at what the intensity of the unwanted stellar light is at the tip of the SMF granted that the light coupled is minimized. A detailed explanation of this method can be found in Llop-Sayson et al. (2019).[9]

One of the main problems with EFC-SMF is the high sensitivity to tip and tilt (T/T) errors. The nature of the null solution that this method achieves is severely sensitive to T/T misalignments, see Fig. 5 in Llop-Sayson et al. (2019).[9] However, this is mostly true when the converged solution for the DM applies a first-order null in the image plane; a second, or higher, order null has shown to be more robust to T/T errors.[12] We are currently working on forcing EFC-SMF to automatically produce second-order nulls in all solutions. For a detailed analysis of low-order wavefront error sensitivity in EFC-SMF solutions see Coker et al. (2019).[7]

4. NARROWBAND EXPERIMENTS

Narrowband EFC-SMF is the preliminary test before performing broadband wavefront control. The experiments presented in this section are done by performing EFC-SMF with a single wavelength, with HCST's tunable filter set to its minimum bandpass, which is measured to be 6nm, thus ∼1% at 780 nm, the center wavelength. The single degree-of-freedom, one control element given that we work with one SMF and one wavelength, allows for a theoretically extreme null solution. Simulations show that monochromatic EFC-SMF go easily beyond 10^{-11} raw contrast for realistic wavefront aberrations.[9] However, in testbed experiments, the effects of PSF jitter limit the achievable performance.

To run the EFC-SMF experiments we use the Matlab Fast Linear Least-Squares Coronagraph Optimization (FALCO) software package[13*], an open source toolbox to run testbeds, perform simulations, and do coronagraph architecture design. One of the main advantages to using FALCO is the rapid computation of the Jacobian, as well as its modularity to perform simulations and run wavefront control on any testbed.

Before running the EFC-SMF wavefront control test, and given the sensitivity to T/T errors, we run conventional EFC over the area surrounding the tip of the SMF in the image plane. We find that the noise induced by the PSF jitter is improved if the intensity over the tip of the SMF is reduced. We dig a dark hole (from 6 to 10 λ/D in a 60° annulus) and reach a level of 10^{-8} raw contrast. Although the solution degrades over the days, the normalized intensity measured through the SMF remains at the level of 10^{-7}.

We present the results of these tests in terms of *normalized intensity*, which we define as the ratio of the intensity measured through the SMF at the image plane after correction, divided by the intensity measured through the SMF with the pseudo-star's PSF centered at the SMF, with the focal plane mask out (> 15 λ/D away), and with the DM shape optimized to the maximum coupling of the HCST's PSF through the SMF.

4.1 Results and Discussion

Fig. 2 shows the normalized intensity over 20 EFC-SMF iterations for a set of ten consecutive EFC-SMF runs. The tip and tilt errors induced by PSF jitter and drift cause the difference between runs to be considerable. However, the algorithm consistently achieves normalized intensities lower than 10^{-8}, although it fails to maintain that low of a contrast for long. The DM solution shape is identical to the simulations solutions, and, as predicted by simulations, the stroke RMS is very low. This is without counting the DM solution applied as the starting DM map to reduce the overall intensity on the SMF tip, as seen in Sec. 4. In Fig. 3, we show an example for a coronagraphic-PSF after the EFC-SMF correction, and its corresponding DM solution.

*https://github.com/ajeldorado/falco-matlab

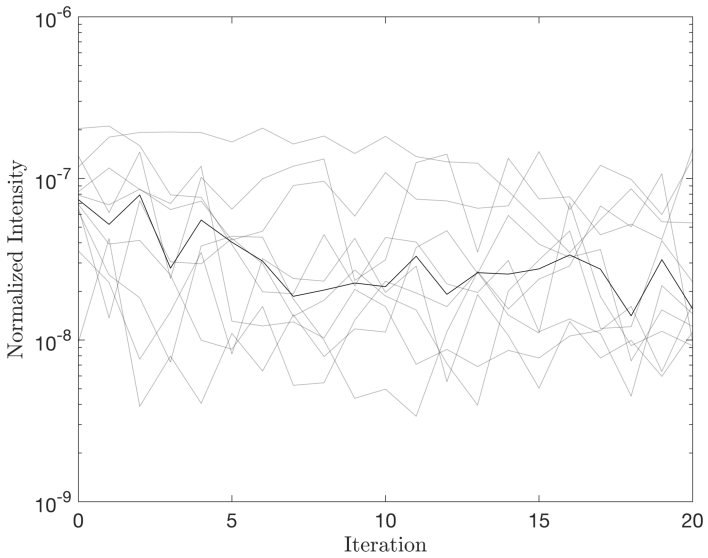

Figure 2. 20-iteration consecutive runs with EFC over an SMF (grey lines). The full color line represents the median of the normalized intensity in every iteration. Tip and tilt errors are the main cause for the deviation between runs. However, the wavefront control algorithm achieves levels of contrast beyond 10^{-8}. Improvements on the PSF jitter and drift problem in HCST will likely boost the EFC-SMF performance in terms of attainable contrast and consistency.

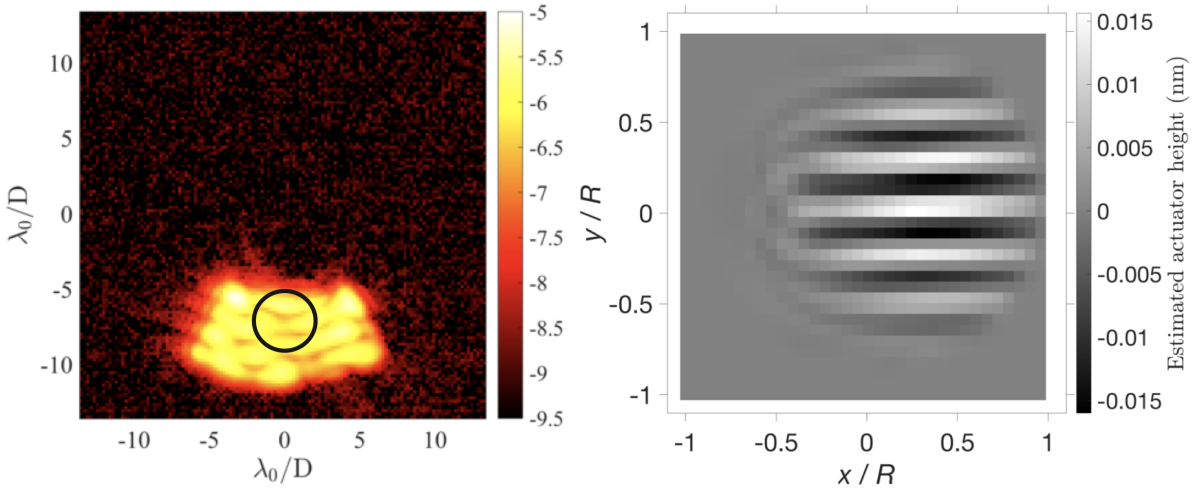

Figure 3. *Left*: Narrowband coronagraphic-PSF after performing wavefront control over the SMF. Although the intensity is two orders of magnitude higher than what measured through the SMF, since the control algorithm is modifying the phase, the coupling through the SMF is nulled to levels of $10^{-8}$and beyond. The field stop blocks most of the light except for a 60° aperture. The black circle indicates the position of the fiber tip. *Right*: Corresponding DM shape solution. The actuator heights are estimated to be very low.

T/T errors, which have been identified as the main limiting factor, can be traced to several causes: (1) PSF jitter caused by air fluctuation in the testbed, (2) PSF drift caused by temperature changes, (3) jitter from vibrations from HCST mechanisms, or external sources such as traffic, (4) loose optics. While some of these can be directly mitigated, this kind of obstacles are part of an in-air testbed. A way to directly reduce PSF motion is by adding a T/T control loop; a steering piezo actuator manufactured by Physics Instrument (PI) is already available in the laboratory. Another way of dealing with this issue is running EFC over a set of random positions in the vicinity of the SMF tip. This allows for an average solution that is more robust to position errors and

thus to PSF jitter and drift. FALCO already has implemented this option to correct for low order aberrations of an arbitrary intensity.

Nevertheless, the problem we are more interested in, the broadband EFC problem, is intrinsically less prone to T/T errors with respect to monochromatic EFC. A single wavelength, over a single position, results in phase-slope solutions in the image plane that are more susceptible to small changes of the SMF's position with respect to the induced slope. A broadband EFC solution is an average solution over a number of wavelengths. This problem converges to a more robust DM shape, generally less sensitive to T/T errors; our simulations show that when comparing identical EFC-SMF runs just changing from one- to multi-wavelength problems, the one-wavelengths solution is significantly (several orders of magnitude) worse in the presence of T/T errors.

Another important limitation is the least-significant bit (LSB) problem. It has been shown that EFC-SMF requires significantly less work from the DM than conventional EFC,[7,9] and attention has to be made to the fact that certain details or characteristics of the shape solution may be lost by the lack of DM actuator stroke resolution. This resolution is driven by the LSB of the controller electronics. The DM solution in Fig. 3 shows estimated strokes of ~ 0.01 nm, which is probably close to the LSB limit. The actual LSB limit and the actuator strokes at low voltages are hard to predict given the non-linearity of the voltage versus actuator height of the DM. The DM vendor specifications show that the non-linearity is accentuated at low voltages. We thus warn that the stroke heights presented here could be rather different to what they really are. From our own interferometric measurements of the DM and from the DM specifications, we estimate that the LSB limit is between 0.007 and 0.1 nm. However, as it is the case with conventional EFC, the broadband DM solution always has higher stroke RMS, from which we surmise that the LSB will be less limiting in the broadband case.

5. TOWARD BROADBAND EFC-SMF

In this section we discuss the steps we are taking toward doing EFC-SMF over a 20% bandwidth.

Broadband wavefront control with conventional EFC was demonstrated in HCST at 10% bandwidth over a clear open aperture pupil,[2] and over the apodized vortex coronagraph prototype apodizer[3] achieving levels of 10^{-8} raw contrast. While these experiments could not reach the level of suppression of 1×10^{-8} that was achieved at narrowband light, the testbed setup has been upgraded significantly, namely by the addition of the field stop (see Sec.2). This, combined with the mode filter nature of the SMF and the power of the adapted wavefront control algorithm, lead us to aim at reaching 1×10^{-8} raw contrast through the SMF at 20% bandwidth.

The VARIA tunable filter was recently characterized, and the wavelength range was checked from 620 nm to 830 nm. The minimum bandpass is consistently $\sim$6 nm. The Thorlabs Optical Spectrum Analyzer (OSA) was used to do this characterization.

As a stepping stone to go to broader bandwidths, we have performed wavefront control experiments at 10% bandwidth. The need for multiple wavelengths significantly increases the control iteration times. The performance is thus penalized by the PSF drift: longer iteration times cause that the slow motion of the PSF in the image plane degrades in a greater way the control from iteration to iteration. However, and although this work is still in progress, we have reached a normalized intensity of 1×10^{-8}. In Fig. 4 we show the coronagraphic-PSF after performing EFC-SMF over 10% bandwidth.

This result, and the results shown in Sec. 4.1, are very encouraging, and, provided that the PSF jitter and drift can be mitigated, we are confident that the 1×10^{-8} raw contrast over a 20% bandwidth milestone is readily achievable.

6. CONCLUSIONS

We have demonstrated the electric field conjugation algorithm adapted to a single mode fiber (SMF) in HCST, and reached consistently levels of a 1×10^{-8}, and beyond. The problems associated with tip and tilt errors discussed in Sec. 4.1 are believed to be the main limitation to this algorithm's performance. However, these can be mitigated to an extent, e.g. with a tip/tilt control loop. In Sec. 5, we showed that we possess the right tools to be able to reach high contrast over an SMF at 20% bandwidth. Our goal of achieving 1×10^{-8} raw contrast at such bandwidths would be an enormous milestone for the direct imaging community. Indeed, this

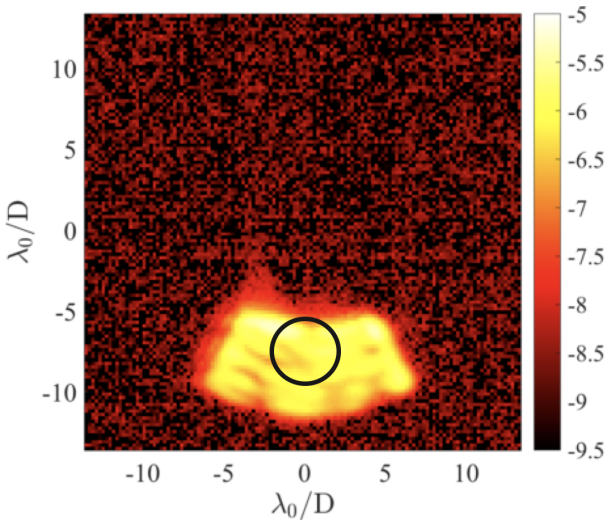

Figure 4. Broadband coronagraphic-PSF (10% at 780 nm) after wavefront correction using the EFC algorithm adapted for an SMF. The intensity is high at the fiber's input, but the phase is asymmetric, which causes the coupling of light into the fiber to null. The field stop blocks most of the light except for a 60° aperture. The black circle indicates the position of the fiber tip.

result would pave the way for going to larger bandpasses and reaching deeper contrast in a vacuum environment; demonstrating a technology that will enable future space missions, such as mission concepts LUVOIR and HabEx, to obtain spectra and detect molecules in other Worlds' atmospheres.

ACKNOWLEDGMENTS

This work was partially supported by the National Science Foundation AST-ATI Grant 1710210.

REFERENCES

[1] Ruane, G., Mawet, D., Delorme, J.-R., Jovanovic, N., Echeverri, D., Llop-Sayson, J. D., Zhang, M. R., Riggs, A. J. E., Shaklan, S., Serabyn, E., and Wallace, J. K., "Laboratory testing of coronagraphs for future space telescopes on the Caltech high contrast spectroscopy testbed for segmented telescopes (HCST) (Conference Presentation)," in [*Space Telescopes and Instrumentation 2018: Optical, Infrared, and Millimeter Wave*], Lystrup, M., MacEwen, H. A., Fazio, G. G., Batalha, N., Siegler, N., and Tong, E. C., eds., **10698**, International Society for Optics and Photonics, SPIE (2018).

[2] Llop-Sayson, J., Ruane, G., Jovanovic, N., Mawet, D., Echeverri, D., Riggs, A. J. E., Coker, C. T., Morrissey, G., and Sun, H., "The high-contrast spectroscopy testbed for segmented telescopes (hcst): new wavefront control demonstrations," (2019).

[3] Llop-Sayson, J., Ruane, G., Mawet, D., Jovanovic, N., Coker, C. T., Delorme, J.-R., Echeverri, D., Fucik, J., Riggs, A. J. E., and Wallace, J. K., "High-contrast demonstration of an apodized vortex coronagraph," *The Astronomical Journal* **159**, 79 (feb 2020).

[4] Ruane, G., Jewell, J., Mawet, D., Pueyo, L., and Shaklan, S., "Apodized vortex coronagraph designs for segmented aperture telescopes," in [], *Society of Photo-Optical Instrumentation Engineers (SPIE) Conference Series* **9912**, 99122L (Jul 2016).

[5] Wang, J., Mawet, D., Ruane, G., Hu, R., and Benneke, B., "Observing Exoplanets with High Dispersion Coronagraphy. I. The Scientific Potential of Current and Next-generation Large Ground and Space Telescopes," *Astron. J.* **153**, 183 (Apr. 2017).

[6] Mawet, D., Ruane, G., Xuan, W., Echeverri, D., Klimovich, N., Randolph, M., Fucik, J., Wallace, J. K., Wang, J., Vasisht, G., Dekany, R., Mennesson, B., Choquet, E., Delorme, J.-R., and Serabyn, E., "Observing Exoplanets with High-dispersion Coronagraphy. II. Demonstration of an Active Single-mode Fiber Injection Unit," *Astrophys. J.* **838**, 92 (2017).

[7] Coker, C. T., Shaklan, S. B., Riggs, A. J. E., and Ruane, G., "Simulations of a high-contrast single-mode fiber coronagraphic multiobject spectrograph for future space telescopes," *Journal of Astronomical Telescopes, Instruments, and Systems* **5**(4), 1 – 14 (2019).

[8] Give'On, A., "A unified formailism for high contrast imaging correction algorithms," *Proc. SPIE* **7440**, 74400D (2009).

[9] Llop-Sayson, J., Ruane, G., Mawet, D., Jovanovic, N., Calvin, B., Levraud, N., Roberson, M., Delorme, J.-R., Echeverri, D., Klimovich, N., and Xin, Y., "Demonstration of an electric field conjugation algorithm for improved starlight rejection through a single mode optical fiber," *Journal of Astronomical Telescopes, Instruments, and Systems* **5**(1), 1 – 11 – 11 (2019).

[10] Foo, G., Palacios, D. M., and Swartzlander, G. A., "Optical vortex coronagraph," *Opt. Lett.* **30**, 3308–3310 (2005).

[11] Mawet, D., Riaud, P., Absil, O., and Surdej, J., "Annular Groove Phase Mask Coronagraph," *Astrophys. J.* **633**, 1191–1200 (2005).

[12] Por, E. H. and Haffert, S. Y., "The Single-mode Complex Amplitude Refinement (SCAR) coronagraph: I. Concept, theory and design," *arXiv e-prints* (Mar. 2018).

[13] Riggs, A. J. E., Ruane, G., Sidick, E., Coker, C., Kern, B. D., and Shaklan, S. B., "Fast linearized coronagraph optimizer (FALCO) I: a software toolbox for rapid coronagraphic design and wavefront correction," in [*Space Telescopes and Instrumentation 2018: Optical, Infrared, and Millimeter Wave*], *Society of Photo-Optical Instrumentation Engineers (SPIE) Conference Series* **10698**, 106982V (Aug. 2018).